Physica A 445 (2016) 57–65

Contents lists available at ScienceDirect

Physica A

journal homepage: www.elsevier.com/locate/physa

# Reservoir characterization using multifractal detrended fluctuation analysis of geophysical well-log data

D. Subhakar, E. Chandrasekhar *

*Department of Earth Sciences, Indian Institute of Technology Bombay, Powai, Mumbai-76, India*

## HIGHLIGHTS

- Represented the fractal scaling exponents in the form of contour plots.
- Role of shale volume in multifractality of different gamma-ray logs is explained.
- Presence of gas in reservoir zones weakens the multifractal behaviour of logs.
- Observed multifractality is due to the presence of long-range correlations in data.

## ARTICLE INFO

*Article history:*
Received 27 April 2015
Received in revised form 25 September 2015
Available online 3 November 2015

*Keywords:*
Multifractal detrended fluctuation analysis
Reservoir characterization
Geophysical well-logs
Bombay offshore basin, India

## ABSTRACT

The spatio-temporal variations in geophysical well-log signals, which often reflect their scale invariant properties, can be well studied with multifractal analysis. In this study, we have carried out fractal and multifractal studies using detrended fluctuation analysis (DFA) and multifractal DFA (MFDFA) respectively. While the DFA primarily facilitates to understand the intrinsic self-similarities in non-stationary signals like well-logs by determining the fractal scaling exponents in a modified least-squares sense, the MFDFA, which in fact, is a generalization of DFA, provides a comprehensive understanding of the multifractal behaviour of the signals through multifractal singularity spectrum as well as the Hurst exponents. DFA and MFDFA have been applied to gamma-ray log and neutron porosity logs of two wells (well B and well C), located in the western offshore basin, India, to study the nature of the subsurface formation properties, vis-à-vis their multifractal behaviour. The estimated DFA fractal scaling exponents, represented in the form of contour plots enable easy identification of the depths to the tops of reservoir zones. On the other hand, the multifractal singularity spectra provide a unique platform for an improved interpretation of logs in terms of their sedimentation pattern and lithological differences. This has been tested with gamma-ray log data of wells B and C. We show that the multifractal behaviour of gamma-ray log is largely influenced by the presence of shale and variations in the subsurface sedimentation pattern. Similarly, the role of gas in a pay zone on the multifractal behaviour was established by comparing the multifractal singularity spectra of the original neutron porosity log and a synthetic neutron log (which we call gas-corrected log), generated using density log. The MFDFA of only that portion of the original neutron log representing the pay zone and its gas-corrected equivalent unequivocally suggest that the presence of gas in the reservoir zones weakens the multifractal behaviour of neutron porosity logs. This emphasizes the significance of multifractal studies of well-logs for effective reservoir characterization. The observed multifractal behaviour in all logs is found to be due to the presence of long-range correlations in the data.



* Corresponding author.
*E-mail address:* esekhar@iitb.ac.in (E. Chandrasekhar).

http://dx.doi.org/10.1016/j.physa.2015.10.103
0378-4371/

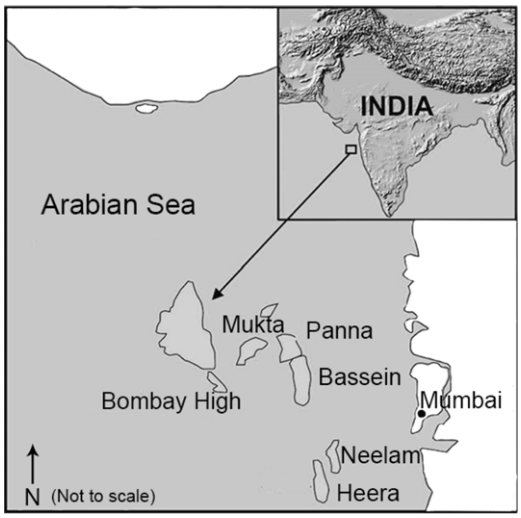


**Fig. 1.** Geographical location of the Bombay High and its contiguous regions in the western offshore basin, India. The data for the present study has been procured from this region (after Chandrasekhar and Rao [1]).

## 1. Introduction

Over the past few decades, geophysical well-log data analyses have witnessed a steady progress, right from the early visual inspection methods to the development of new and fast data analysis techniques for better understanding of the subsurface formations in a broader perspective (see Chandrasekhar and Rao [1] and references therein for complete details of chronological history of developments in various mathematical techniques for well-log data analysis). Among the several techniques developed, wavelet analysis (WA) has been proven to be one of the most efficient ones for providing the space-localization of different subsurface formations. WA has found its wide applications in effectively describing the inter-well relationship [2], determining the sedimentary cycles [3], reservoir characterization [4,5] and for determining the space-localization and identifying the depths to the tops of formations [1].

It has been recognized that the well-log data display multifractal behaviour and thus can be aptly studied to understand such behaviour that has links to the physical properties of the subsurface formations. Khue et al. [6] applied a generalized multifractal analysis to study classification of sediment formations. Lopez and Aldana [7] made a wavelet-based fractal analysis of well-log data for facies recognition and classified different formations based on their fractal dimension. Ouadfeul and Aliouane [8] carried out DFA and multifractal analysis of well-logs by using wavelet transform modulus maxima method for segmentation of lithofacies. Hernandez-Martinez et al. [9] applied Detrended Fluctuation Analysis (DFA) to well-log data for identification of facies associations. Chandrasekhar and Dimri [10] described a methodology for wavelet-based fractal analysis of geophysical data.

In the present study, we apply DFA and multifractal DFA (MFDFA) technique to gamma-ray log and neutron porosity log data sets of two wells located off the west-coast of India, to (i) identify the depths to the tops of formations and compare the results of DFA and wavelet analysis, (ii) characterize different properties of subsurface formations based on the multifractal behaviour of well-log data and (iii) understand whether the multifractal behaviour in well-log signals is due either to the presence of long-range correlations or the broad probability distribution in the data. The organization of the chapter is as follows. Section 2 briefly describes the geology of the study area and the data used in the present study. Section 3 discusses the basic theory and mathematical details of DFA and MFDFA techniques. Section 4 describes the application of DFA and MFDFA to the present data. Section 5 provides the results and discussion of the interpretation of the results. Section 6 provides the conclusions of the present study.

## 2. Geology of the study area and data

Fig. 1 illustrates the geographical location of the wells off the west coast of India. The subsurface in the study area mainly comprises of L-I, L-II limestone reservoir zones at the top, which are bounded by shales; the S-I gas–sand zone, a mixture of shale–sand in the middle; and L-III, the largest limestone reservoir zone at the bottom, which was deposited due to cyclic sedimentation of shale and limestone (resulting in alternate sequences of shale and limestone facies). Further details about the geology and lithostratigraphy of the study area can be found in Chandrasekhar and Rao [1]. We have used the gamma-ray log and neutron porosity log data sets that were used in Chandrasekhar and Rao [1], but of only two wells, well B and well C.

## 3. MFDFA formulation

Before discussing the MFDFA algorithm, it would be appropriate and worthwhile to understand the DFA process in the first place. The DFA technique was primarily developed as a tool to study the inherent scaling properties in non-stationary signals. Scaling properties provide knowledge about the long-range positive correlations and persistent power-law behaviour of the signal under investigation, which in general, is affected by nonlinearities and long-term/short-term trends. DFA facilitates to characterize the scaling properties in any given signal devoid of non-stationarities in it. For estimation of scaling exponents through DFA, the signal under investigation, which can be converted to a self-similar process by integration [11], should obey the power-law behaviour over various window lengths. Integration would help to unravel the power-law nature by making the signal unbounded and facilitates to detect the underlying self-similarities in the data over various window lengths. The entire description of MFDFA technique in lucid mathematical steps is as follows.

1. First generate an integrated series $y(m)$ of $N$-point spatial data sequence, say, $x(i)$, by estimating

$$y(m) = \sum_{i=1}^{m} (x(i) - \bar{x}); \quad m = 1, 2, 3, \ldots N \tag{1}$$

   $\bar{x}$ designates the mean of the $N$ data points.
2. Next, divide the $m$-length integrated series into various $m/k$ non-overlapping windows of equal length, each consisting of $k$ number of samples. Thus the total number of windows is, $N_k = int(m/k)$.
3. Calculate the least-squares fit of preferred order to the data points in each window. This represents the local trend $y_k$.
4. Detrend the integrated series $y(m)$ by subtracting the local trend $y_k$ from the corresponding window. For a window of length, $k$, calculate the average fluctuations, $F(k, n)$, of the detrended series in forward and backward directions by

$$F(k, n) = \sqrt{\frac{1}{k} \sum_{i=s+1}^{nk} [y(i) - y_k(i)]^2} \tag{2}$$

   where, $s = (n-1)k$; $n$ depicts the window number. $n = 1, 2, 3 \ldots N_k$ for forward operation and $n = N_k,\ N_k - 1,\ N_k - 2 \ldots 3, 2, 1$ for backward operation.
5. Taking into account both forward and backward operations, the generalized form for overall average fluctuations is expressed as $q$th order fluctuation function as [12]

$$F_q(k) = \left\{ \frac{1}{2N_k} \sum_{n=1}^{2N_k} \left[F^2(k, n)\right]^{q/2} \right\}^{1/q}. \tag{3}$$

   Eq. (3) is iteratively calculated for various window lengths, $k$[1] and $q$ values, to provide a power-law relation between $F_q(k)$ and $k^{h(q)}$. The generalized Hurst exponent $h(q)$ defines the slope of the linear least-squares regression between the logarithm of the overall average fluctuations $F_q(k)$ and the logarithm of the window length $k$, for corresponding $q$. Generally, Eq. (3) is calculated for various $q$ ranging from $-10$ to 10. However, for better characterization of the signal, further higher or lower bounds of $q$ can be chosen. For the case of $q = 0$ (as the exponent becomes divergent at this value), Eq. (3) will be transformed to a logarithmic averaging procedure, given by [12]

$$F_0(k) = \exp\left[ \frac{1}{4N_k} \sum_{n=1}^{2N_k} \ln\left\{F^2(k, n)\right\} \right] \approx k^{h(0)}. \tag{4}$$

   The behaviour of multifractal Hurst exponent, $h(q)$ depends on the average fluctuations $F_q(k)$. It bears a non-linear relation with the order of the fluctuation function, $q$, such that the low (high) average fluctuations have high (low) $h(q)$ for negative (positive) $q$ [12]. If $h(q)$ varies (remains constant) for various $q$, then the signal is said to have multifractal (monofractal) behaviour. This can be checked by $h(q)$ vs. $q$ plot.
6. Next, estimate the multifractal singularity spectrum, defining the relation between the singularity spectrum, $f(\alpha)$ and strength of the singularity, $\alpha$, defined by $\alpha = h(q) + qh'(q)$ and $f(\alpha) = q[\alpha - h(q)] + 1$. $\alpha$ is also known as Hölder exponent. The reader is referred to Kantelhardt et al. [12] for more details on $\alpha$ and $f(\alpha)$. The shape of singularity spectrum resembles that of a Gaussian curve. The broader (narrower) the singularity spectrum, the stronger (weaker) the multifractal nature of the signal [14].
7. As explained above, for a limiting case of $q = 2$, $F_q(k)$ (Eq. (3)) estimated only in forward direction defines DFA. The scaling exponents using DFA can be calculated in both non-overlapping and overlapping (also known as sliding window) methods. Particularly, the latter is advantageous in well-log data applications for estimation of depths to the tops of reservoir zones (cf. Section 4.1). Also, the scaling exponent values for the case of $q = 2$ (i.e. $h(2)$) can be examined to

[1] According to Peng et al. [13], the successive window lengths, $k$, are increased by a factor of $2^{1/8}$.

**Table 1**
Comparison of depths to the tops of reservoir zones estimated for different logs from the present study, wavelet analysis [1] and with the known depth estimates provided by ONGC Ltd.

| Well | Zone | Depth estimates obtained from the present study (m) | | Depth estimates obtained by wavelet analysis using Gaus1 wavelet (m) | | Known depth estimates provided by ONGC Ltd. (m) |
|---|---|---|---|---|---|---|
| | | Gamma-ray | Neutron Porosity | Gamma-ray | Neutron Porosity | |
| Well B | L-I | – | – | 983 | 980.2 | 980.5 |
| | L-II | 1006 | 1006 | 1006 | 1008 | 1006 |
| | S-I | 1202 | 1202 | 1200 | 1201 | 1202 |
| | L-III | 1329 | 1329 | 1329 | 1328 | 1329 |
| Well C | L-I | 1004 | 1004 | 1003 | 1004 | 1004 |
| | L-II | 1032 | 1032 | 1031 | 1032 | 1032 |
| | S-I | 1193 | 1193 | 1200 | 1189 | 1195 |
| | L-III | 1361 | 1361 | 1361 | 1361 | 1361 |

understand whether the multifractal behaviour in any signal is due to the presence of long-range correlations or broad probability distribution in the data.

Unlike in non-overlapping window method, the chosen windows are shifted in unit steps in sliding window method. Accordingly, the average fluctuations are estimated by using a modified form of Eq. (2), expressed as, $F(k,n) = \sqrt{\frac{1}{k}\sum_{i=n}^{k+(n-1)}[y(i)-y_k(i)]^2}$, where, $n = 1,\ 2,\ 3\ldots, m-k+1$ and '$m$' is the length of the integrated series. In this method, first a window of chosen length, $k$, is placed at the start of the integrated series (see Eq. (1)) and the scaling exponent, $\gamma_k(n)$, defined as $\gamma_k(n) = \frac{\log(F(k,n))}{\log(k)}$, corresponding to $n$th window of length $k$, will be estimated and attributed to the centre of that window. We call $\gamma_k(n)$ as local scaling exponent. Next the window is shifted by unit distance along the depth axis and the above procedure is repeated to determine the scaling exponent and attributed it to the centre of that position of that window. This is continued till the end of the data is reached. This procedure is repeated for different window lengths. Thus, the continuous shifting of windows along the depth axis for various window lengths is analogous to translation and dilation process in continuous wavelet transform. The thus obtained all the scaling exponents of all the windows are represented in the form a contour plot, depicting the variation of scaling exponents as a function of depth. The contour plot resembles a wavelet scalogram and thus facilitates easy and quick identification of depths to the tops of reservoir zones.

## 4. Application of sliding window DFA and MFDFA to well-log data

### 4.1. Sliding window DFA approach

DFA scaling exponents using sliding window approach were determined for gamma-ray and neutron porosity logs of wells B and C. Here, the minimum and maximum window lengths were considered to be 1.5 m and 30 m respectively, with an increment of 0.75 m in successive window lengths. Beyond these limits, the data were found to be affected largely by artefacts and averaging effects. Fig. 2 depicts the contour plots of local scaling exponents $\gamma_k(n)$ (see Section 3) obtained for various window lengths as a function of depth corresponding to gamma-ray log and neutron log of well B (Fig. 2(a)) and well C (Fig. 2(b)). These contour plots were further used to identify the reservoir boundaries from both the wells. Table 1 explains the depths to the tops of reservoir zones obtained using this study, wavelet analysis [1] and the depth estimates provided by the Oil and Natural Gas Commission (ONGC) Ltd., India.

### 4.2. MFDFA approach

MFDFA has been applied to gamma-ray log and neutron porosity log of wells B and C. To determine the multifractal Hurst exponents for different moments ($q$), a minimum (starting) window length of 1.5 m and a maximum window length of about 125 m (which is equivalent to $(N/4) \times 0.15$ m) were considered. $N$ denotes the total number of data points and 0.15 m is the sampling interval of the data (see Chandrasekhar and Rao [1]). A linear least-squares fit was fit to the data in each window to calculate the local trend for its subsequent removal from each data point of the corresponding window. Following Peng et al. [13], the successive window sizes are incremented by a factor of $2^{1/8}$. Using Eqs. (3) and (4), the multifractal Hurst exponents, $h(q)$, were determined by varying $q$ in the range, $-15$ to 15 for the present data sets. Fig. 3 represents the Hurst exponents (Fig. 3(a)) and multifractal singularity spectra (Fig. 3(b)) corresponding to gamma-ray logs of wells B and C. Fig. 4 represents the Hurst exponents (Fig. 4(a)) and multifractal singularity spectra (Fig. 4(b)) corresponding to neutron porosity logs of wells B and C. The multifractal behaviour of the data can be clearly discerned by observing the broadness in the spectra. The broader the singularity spectra, the higher the multifractality of the data and vice versa.

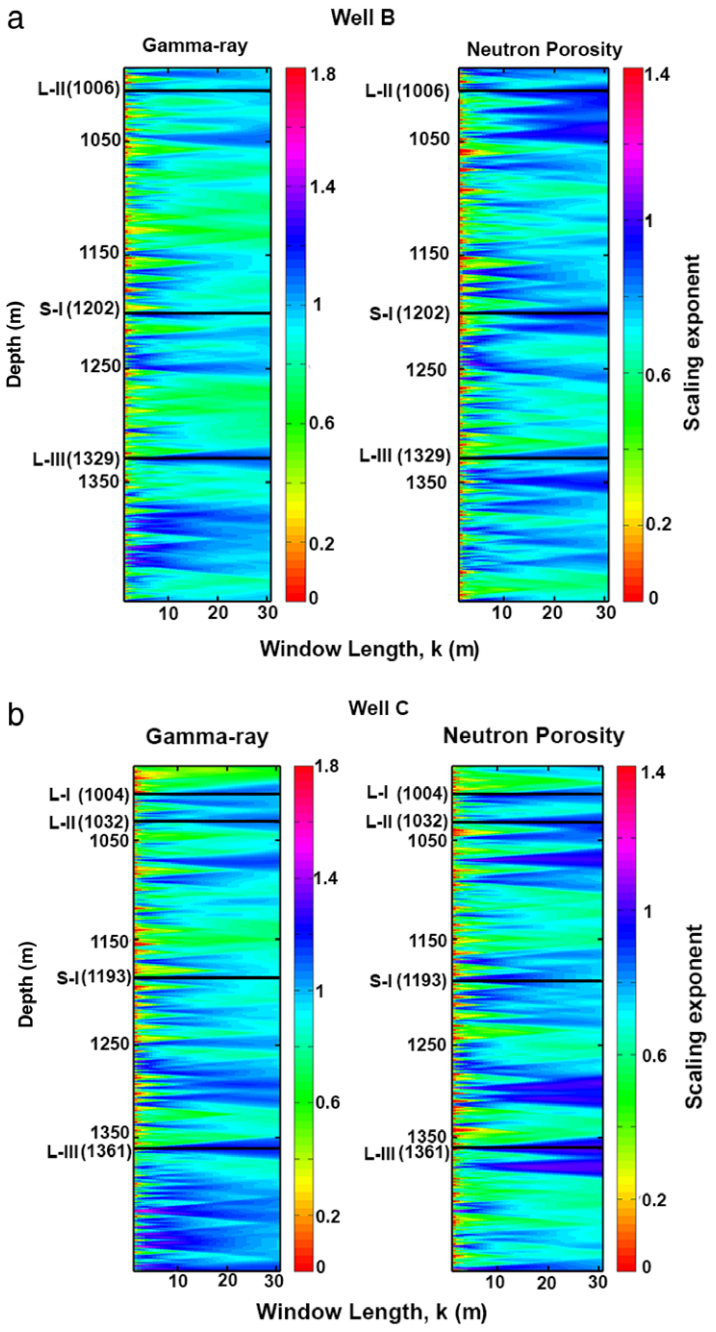


**Fig. 2.** Contour plots of local scaling exponents $\gamma_k(n)$ (see Section 3) obtained for various window lengths as a function of depth, clearly depicting the depth locations of various reservoir zones identified from gamma-ray and neutron porosity logs of (a) well B and (b) well C. (For interpretation of the references to colour in this figure legend, the reader is referred to the web version of this article.)

## 5. Results and discussions

In the study area, the important reservoir zones are L-I, L-II and L-III (limestones) and S-I (gas sand). L-I, L-II and L-III zones have shale as their cap rock and S-I zone is a mixture of sand and shale. Fig. 2 shows a clear demarcation of these different reservoir zones identified based on the variation of local scaling exponents. Fig. 2(a), (b) also shows several other thin layers (indicated in blue colour) located at various depth locations. Such an identification of very thin layers is generally possible when scaling exponents are computed for small window lengths. In this study, we have gradually varied window lengths from the smallest (1.5 m) to largest (30 m) with a very small increment of only 0.75 m for estimation of scaling exponents. This is similar to varying the wavelet scales from low to high in wavelet analysis of the same data sets, whose results also

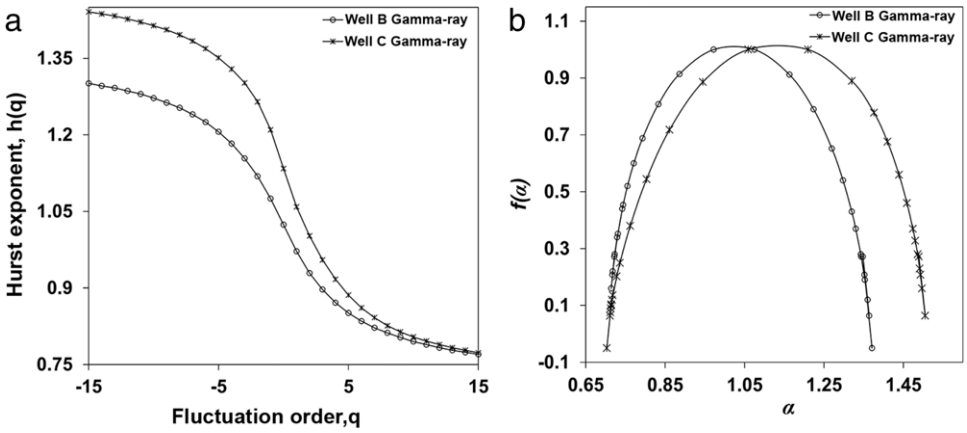


**Fig. 3.** (a) The $q$ dependence of generalized Hurst exponents, $h(q)$ determined for gamma-ray logs of well B (open circles) and well C (stars). (b) Multifractal singularity spectra for gamma-ray logs of well B (open circles) and well C (stars). The solid lines in both plates depict the lines joining the points of respective curves. Note the spectrum depicting Gaussian shape to be narrow for well B compared to that of well C, indicating the weaker multifractality in gamma-ray log of well B.

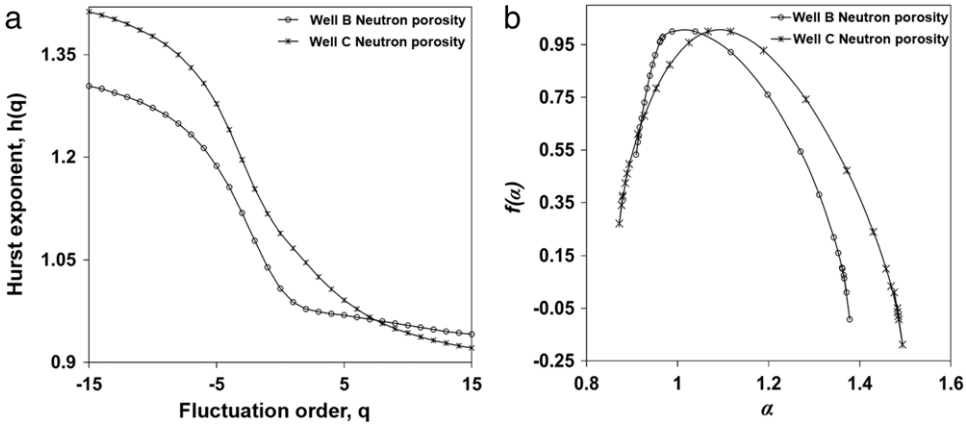


**Fig. 4.** Same as Fig. 3, but for neutron porosity logs.

show these thin layers (see Chandrasekhar and Rao [1]). However, the lithological details of these identified thin layers were not available for further examination. Generally, at the depths demarcating these shale–limestone boundaries (L-I, L-II and L-III) (Fig. 2), the average fluctuations, $F(k, n)$, corresponding to each log increase due to variation in the respective physical property. For example, in gamma-ray logs, the natural radioactivity for shales is high compared to that of sand and limestones. Accordingly, at the shale–limestone and at shale–sand boundary, the demarcation is clearly seen. Neutron porosity logs indicate the measure of hydrogen index of the formation, which is directly proportional to the neutron porosity. While neutron porosity is low in reservoir zones due to low hydrogen index, it is high in shales due to the presence of bound water. However, in case of rocks filled with gas, the neutron porosity values are much lower than the same rock filled with oil or water. When such gas zones are overlain/underlain by shales, the high neutron porosity of shales results in increase in the average fluctuations. As a result, the average fluctuations and local scaling exponent values increase across the shale–sand or shale–limestone reservoir boundaries. Thus, in both the wells, the spatial locations of limestone and sand reservoir zones could be clearly delineated with high resolution, due to significant differences in the respective physical properties of reservoir zones.

The multifractal Hurst exponent curves of gamma-ray logs of wells B and C (Fig. 3(a)) show a large separation between them for negative $q$, which gradually decreases with increase in $q$ and almost merge with each other at the positive highest $q$. We have earlier mentioned that high average fluctuations in the data yield low Hurst exponent values (see point # 5 in Section 3). In Fig. 3(a), since the Hurst exponents are low for well B than well C, the average fluctuations for the former are high compared to the latter. Probably, this could be due to high amount of shale deposition in well B than in well C. This is verified by estimating the shale volume ($V_{sh}$) from the entire gamma-ray log and also from the zone-wise analysis of gamma-ray log data of both wells, using the formula, $\mathrm{V_{sh}} = \frac{GR - GR_{\min}}{GR_{\max} - GR_{\min}}$ [15], where, $GR$ refers to gamma-ray log values. The overall shale volume for well B is estimated to be 51%, while that for well C is 44%. In the zone-wise analysis, the shale volume corresponding to L-III zone of well B is 20%, while that for well C is 9%. The multifractal singularity spectra of gamma-ray

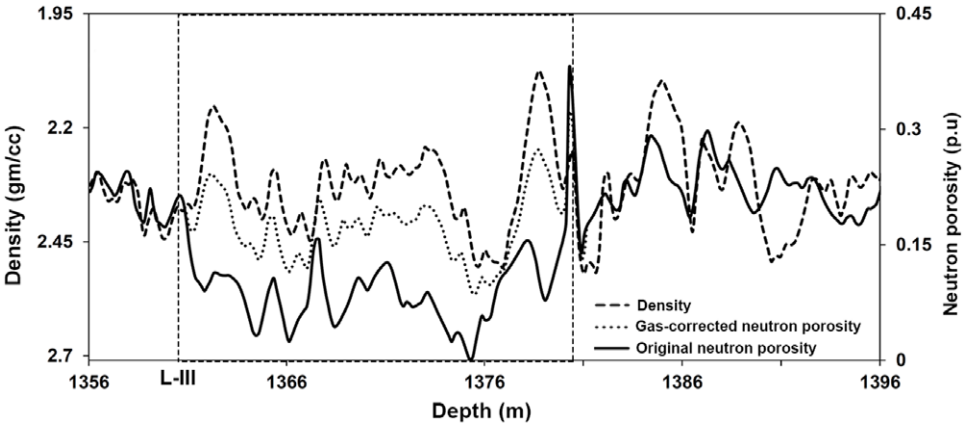


**Fig. 5.** Cross-over of neutron porosity log (solid line) and density log (dashed line) corresponding to the L-III pay zone of well C. The highlighted portion of the data (shown in the dashed box) signifies a characteristic of the presence of a continuous thick gas column of about 20 m in this zone, which shows a narrow multifractal singularity spectrum (see Fig. 6). The dotted line portion of the data in L-III zone depicts the gas-corrected neutron porosity.

logs of both the wells show the singularity spectrum of well B is slightly narrower than that of well C (Fig. 3(b)). The spectral width reflects the degree of multifractality or heterogeneity in sedimentation pattern in the wells and thus the narrower (broader) spectrum of well B (well C) indicates a lower (higher) heterogeneity dominated by high (low) shale deposition.

Similar to those of gamma-ray logs, the Hurst exponent values of neutron porosity log of well B are smaller than those of well C (Fig. 4(a)). Interestingly, for well B, they tend to become almost constant for all positive $q$, while the situation is not similar in case of well C. This indicates the absence of large average fluctuations in neutron porosity in well B and the presence of combined large and small average fluctuations in neutron porosity in well C. Accordingly, the respective singularity spectra (Fig. 4(b)) also show a slightly narrower spectrum for well B and broader spectrum for well C. It can be generally argued that while the small average fluctuations suggest the presence of thick homogeneous zones, the large average fluctuations arise due to significant differences in neutron porosity values.

The limestone L-III pay zone is the largest reservoir zone in the study region. A visual observation of neutron and density logs of both wells indicated the presence of a continuous and thick gas column of about 20 m in L-III zone in well C, while the gas in L-III zone is present intermittently in well B and thus the scenario in the L-III zone of both wells is different. Therefore, it is worthwhile to have a greater insight into the multifractal behaviour of the largest L-III pay zone and its influence on the overall multifractal behaviour of the entire log of well C. A comparison of neutron porosity and density logs of L-III zone clearly shows some distinct phase differences between them within the depth range of about 1360 m and 1380 m (see the portion of the logs highlighted in dashed box in Fig. 5). The density and neutron porosity values are distinct because of low density and low hydrogen index. To understand the effect of the gas, on the multifractal behaviour of neutron porosity of L-III zone of well C, the highlighted portion of the data in Fig. 5 has been corrected for gas using the formula, $\phi_C = \sqrt{\frac{\phi_N^2+\phi_D^2}{2}}$, where $\phi_N$ denotes the neutron porosity value and $\phi_C$ represents the neutron porosity values corrected for gas. The density porosity log ($\phi_D$) has been generated with limestone matrix density ($\rho_{matrix}$) of 2.71 gm/cc and fluid density ($\rho_{fluid}$) of 1.0 gm/cc using the formula $\phi_D = \frac{\rho_{matrix}-\rho_{bulk}}{\rho_{matrix}-\rho_{fluid}}$ [15]. Next, the original neutron porosity log of L-III zone of well C and its gas-corrected portion were subjected to MFDFA. The multifractal singularity spectra of both these logs shown in Fig. 6, clearly describe that the spectrum of the original neutron porosity log is narrow compared to that of the gas-corrected zone, which is broad, suggesting a stronger multifractality in the latter. In other words, the presence of gas in the reservoir zones weakens the multifractal behaviour of neutron porosity logs. Analysing synthetic seismic data, Khan and Fadzil [16] also explain that the gas in reservoir zones exhibits weak multifractality. However, the effect of gas-corrected portion of the neutron porosity values on the multifractal behaviour of the entire log is not significant (not shown here). This unequivocally confirms that zone-wise MFDFA studies of well-logs are rather important and essential to understand the multifractal behaviour of the logs in a broader perspective, for effective reservoir characterization.

The observed multifractal behaviour of the logs could be either due to the presence of long-range correlations or the broad probability distribution of the data. This can be checked by shuffling the original data sequence. By shuffling, we make the data series random and thus the long-range correlations present (if any) in it will be destroyed. If the scaling exponent for the shuffled data (i.e. uncorrelated random noise) is equal to 0.5, then the observed multifractality is due to long-range correlations present in the original data. Otherwise, it is due to broad probability distribution in the data [11]. Examination of the scaling exponent values estimated for all logs and their shuffled sequences for the case of $q = 2$ (see point # 7 in Section 3) lay in the range of 0.48–0.51. Fig. 7 shows an example of the multifractal singularity spectra of gamma-ray log of well B and its shuffled sequence. Inset in Fig. 7 represents the scaling exponent, $h(2)$ (slope), derived for the shuffled sequence. The scaling exponent value of 0.51 coupled with the very narrow singularity spectrum of the shuffled sequence

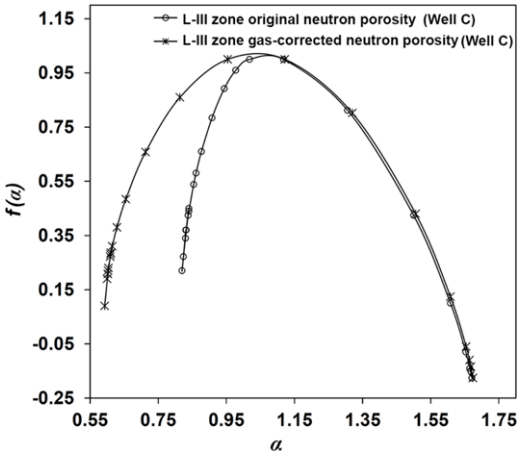


**Fig. 6.** Multifractal singularity spectra of the original neutron log of L-III pay zone of well C (open circles) and its gas-corrected equivalent (stars). The respective data are shown as solid line and dotted line in Fig. 5. Note the spectra depicting the Gaussian shape to be narrow for the former (suggesting weak multifractality) and broad for the latter (suggesting strong multifractality).

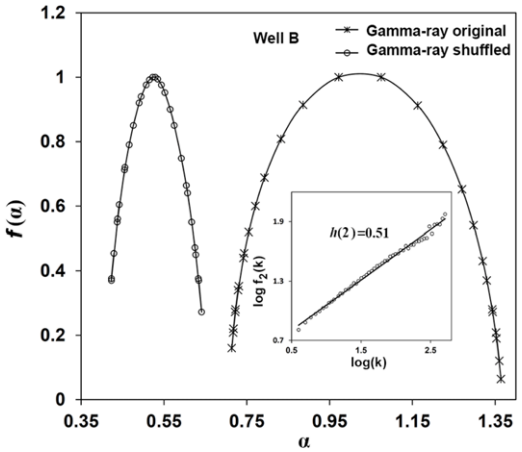


**Fig. 7.** Multifractal singularity spectra of gamma-ray log (stars) and its shuffled sequence (open circles) of well B. Inset shows the scaling exponent, $h(2)$ determined for the shuffled sequence (see text for more details).

confirms that the multifractal behaviour of all the logs is solely due to the presence of long-range correlations and not due to the broad probability distribution in the data.

## 6. Conclusions

The following conclusions are drawn from our present study.

1. For the first time we have represented the fractal scaling exponents of different windows in the form of contour plots to effectively delineate the depths to the tops of reservoir zones. The thus identified depths match well with those of wavelet analysis [1] and with those provided by ONGC Ltd.
2. The overall multifractal behaviour of well B is weaker than that of well C, corresponding to all the logs, as evident from the respective low Hurst exponent values and narrow singularity spectra.
3. We have clearly identified that the weaker multifractality in gamma-ray log of well B (i.e., low Hurst exponent values and narrow singularity spectrum) compared to that of well C to be due to the large shale volume in well B than in well C. Using gamma-ray log data, we have estimated the shale volume in well B to be 51% and in well C to be 44% for the entire log and 20% (well B) and 9% (well C) in the largest L-III pay zone only.
4. Again for the first time, through well-log data analysis, we have shown that the presence of a continuous and thick gas volume in the reservoir zones displays a narrow multifractal singularity spectrum, suggesting a weak multifractality in the well-log signals. This largely confirms that the zone-wise MFDFA studies of well-logs are rather important and essential to understand the multifractal behaviour of the logs in a broader perspective, for effective reservoir characterization.

5. The overall multifractal behaviour in all the logs of both wells is found out to be due to the presence of long-range correlations in the data and not due to the broad probability distribution.

## Acknowledgements

The authors thank Oil and Natural Gas Commission Ltd., India, for providing the necessary data and for their permission to publish this work. The authors also thank the handling editor, H. E. Stanley and an anonymous referee for their meticulous reviews, which have improved the quality of the paper.

## References

[1] E. Chandrasekhar, V.E. Rao, Wavelet analysis of geophysical well-log data of Bombay offshore basin, India, Math. Geosci. 44 (2012) 901–928.
[2] F.E. Jansen, M. Kelkar, Application of wavelets to production data in describing inter-well relationships, in: Soc Petr Engr # 38876: Annual Technical Conference and Exhibition, San Antonio, TX, October 5–8, 1997.
[3] A. Prokoph, F.P. Agterberg, Wavelet analysis of well-logging data from oil source rock, Egret Member offshore eastern Canada, Am. Assoc. Pet. Geol. Bull. 84 (2000) 1617–1632.
[4] M.N Panda, C.C Mosher, A.K. Chopra, Application of wavelet transforms to reservoir—data analysis and scaling, SPE J. 5 (2000) 92–101.
[5] N.R. Vega, Reservoir characterization using wavelet transforms (Ph.D. dissertation), Texas A&M University, USA, 2003.
[6] P.N. Khue, O. Housby, A. Saucier, J. Muller, Application of generalized multifractal analysis for characterization of geological formations, J. Phys.: Condens. Matter. 14 (9) (2002) 2347–2352. http://dx.doi.org/10.1088/0953-8984/14/9/323.
[7] M. Lopez, M. Aldana, Facies recognition using wavelet based fractal analysis and waveform classifier at the Oritupano-A field, Venezuela, Nonlinear Process. Geophys. 14 (2007) 325–335.
[8] S.A. Ouadfeul, L. Aliouane, Multifractal analysis revisited by the continuous wavelet transform applied in lithofacies segmentation from well-logs data, Int. J. Appl. Phys. Math. 1 (1) (2011) 10–17.
[9] E. Hernandez-Martinez, Jorge X. Velasco-Hernandez, Teresa Perez-Muñoz, Jose Alvarez Ramirez, A DFA approach in well-logs for the identification of facies associations, Physica A 392 (2013) 6015–6024.
[10] E. Chandrasekhar, V.P. Dimri, Introduction to wavelets and fractals, in: E. Chandrasekhar, V.P. Dimri, V.M. Gadre (Eds.), Wavelets and Fractals in Earth System Sciences, CRC Press, Taylor and Francis Group, U.K, 2013, pp. 1–27.
[11] A.L. Goldberger, L.A.N. Amaral, L. Glass, J.M. Hausdorff, P.Ch. Ivanov, R.G Mark, J.E Mietus, G.B Moody, C.-K. Peng, H.E. Stanley, Physio bank, physio toolkit, and physio net: Components of a new research resource for complex physiologic signals, Circulation 101 (23) (2000) e215–e220. http://circ.ahajournals.org/cgi/content/full/101/23/e215.
[12] J.W. Kantelhardt, S.A. Zschiegner, E. Koscielny-Bunde, A. Bunde, S. Havlin, H.E. Stanley, Multifractal detrended fluctuation analysis of nonstationary time series, 2002, pp. 1–9. Preprint, arXiv:physics/0202070v1.
[13] C.K. Peng, S.V. Buldyrev, M. Simons, H.E. Stanley, A.L. Goldberger, Mosaic organization of DNA nucleotides, Phys. Rev. E 49 (1994) 1685–1689.
[14] M.J.A. Bolzan, A. Tardelli, V.G. Pillat, P.R. Fagundes, R.R. Rosa, Multifractal analysis of vertical total electron content (VTEC) at equatorial region and low latitude, during low solar activity, Ann. Geophys. 31 (2013) 127–133. http://dx.doi.org/10.5194/angeo-31-127-2013.
[15] S. Jarot, S. Ariffin, Formation evaluation: Correlation between clay volume and porosity based on well logging data, in: Scientific Conference III — Universiti Kebangsaan Malaysia (UKM), 2008. pp. 1–9.
[16] M.M. Khan, M.H.A. Fadzil, Singularity spectrum of hydrocarbon fluids in synthetic seismograms, in: Proc. of Intl. Conf. on Intelligent and Advanced Systems, IEEE Xplore, 2007, pp. 1236–1239. http://dx.doi.org/10.1109/ICIAS.2007.4658581.